Nigerian Journal of Applied Physics (NJAP)
ISSN Print: 3115-5871
ISSN Online: 3115-588X
DOI: https://doi.org/10.62292/njap-v2i2-2026-61
Volume 2(2), June 2026

Cutoff Effects on the Equation of State of a Lennard–Jones Fluid: A Statistical Mechanical Analysis

***Isaiah Eze Igwe and Moses A. Tyav**

Department of Physics, Federal University Dutsin-Ma, Katsina State, Nigeria.

*Corresponding author's email: iigwe@fudutsinma.edu.ng

Keywords:
Lennard–Jones fluid,
Molecular Dynamics simulation,
Equation of state,
Virial pressure,
Cutoff radius,
Thermodynamic properties.

ABSTRACT

The Lennard–Jones (LJ) fluid is a standard model for linking microscopic intermolecular interactions to macroscopic thermodynamic behavior, yet its Molecular Dynamics (MD) predictions remain sensitive to potential truncation. This study uses equilibrium MD simulations to determine the equation of state (EOS) of a three-dimensional LJ fluid across reduced densities and temperatures. Pressure, potential energy, and compressibility factor were computed using the virial formulation, with emphasis on how cutoff radius and analytical tail corrections affect thermodynamic accuracy. The simulations reproduced expected LJ-fluid behavior: pressure increased nonlinearly with density, while the compressibility factor showed a transition from attraction-dominated states ($Z < 1$) to repulsion-dominated states($Z > 1$). Comparing$r_c = 2.0\sigma, 2.5\sigma$, and 3.0σ revealed systematic truncation errors that increased with density. At $T^* = 1.2$ and$\rho^* = 0.8$, pressure deviations between the smallest and largest cutoffs reached about 6–10%, while potential-energy deviations exceeded 10%. Tail corrections substantially reduced these errors and improved agreement with larger-cutoff simulations, although residual deviations persisted in dense, strongly correlated states. The findings show that cutoff treatment is a state-dependent thermodynamic bias in EOS reconstruction, not merely a computational setting.

INTRODUCTION

Simple liquids continue to occupy a central position in statistical mechanics, liquid-state theory, and computational thermodynamics because they provide one of the clearest environments in which microscopic interactions can be connected directly to macroscopic observables(Hansen & McDonald, 2013; McQuarrie, 2000; Rowlinson & Widom, 2002). Yet, despite decades of theoretical and computational development, even the thermodynamic description of apparently simple fluids remains sensitive to implementation details that are sometimes treated as secondary numerical choices rather than physically consequential approximations (Allen & Tildesley, 2017; Daan Frenkel & Smit, 2002a). This tension is particularly evident in Molecular Dynamics (MD) simulations of the Lennard-Jones (LJ) fluid, where quantities such as pressure and internal energy may depend not only on the intermolecular potential itself, but also on how that potential is truncated, shifted, or corrected during numerical evaluation (Gottschalk, 2019; Johnson, Zollweg, & Gubbins, 1993; Thol et al., 2016; Wang, Ramírez-Hinestrosa, Dobnikar, & Frenkel, 2020).

The LJ potential introduced by Jones (1924) remains the most widely studied model potential for simple atomic fluids (Hansen & McDonald, 2013; Jones, 1924). Its persistence within the statistical mechanics literature is not merely historical. Rather, the model provides a compact representation of the balance between short-range Pauli exclusion repulsion and long-range London dispersion attraction that governs the behavior of many nonpolar systems (McQuarrie, 2000; Rowlinson & Widom, 2002). The repulsive r^{-12} contribution prevents unphysical particle overlap, while the attractive r^{-6} term stabilizes condensed phases and drives vapor-liquid coexistence(Hansen & McDonald, 2013; Jones, 1924). Although the potential ignores directional bonding, polarization effects, and many-body electronic contributions, it still reproduces a remarkable range of fluid phenomena with reasonable accuracy (Allen & Tildesley, 2017; Daan Frenkel & Smit, 2002a). For this reason, the LJ fluid has become something of a reference system in computational statistical mechanics. It has been used extensively to study phase equilibria (Alder & Wainwright, 1957; Baidakov, 2022; Sun & Teja, 1998),

transport properties (Allen & Tildesley, 2017; Koplik, Banavar, & Willemsen, 1990), critical phenomena (Panagiotopoulos, Suter, & Reid, 1986; Pang, Wu, Chen, & Pan, 2026), nucleation dynamics (Lutsko, 2019; Ouyang, Sun, Sun, & Xu, 2020), interfacial thermodynamics (Bhatt, Newman, & Radke, 2002; Di Pasquale et al., 2025), and finite-size effects (Rocklin, Mobley, Dill, & Hünenberger, 2013). The model also plays an important role in validating simulation methodologies themselves, since highly accurate reference equations of state and coexistence curves are available for direct comparison. Consequently, even small discrepancies between independent simulations and reference thermodynamic data become scientifically meaningful.

MD simulation provides a direct route for connecting microscopic interactions to thermodynamic properties through deterministic trajectory evolution (Allen & Tildesley, 2017; Ciccotti, Decherchi, & Meloni, 2025; Daan Frenkel & Smit, 2002b). Since the foundational work of Alder and Wainwright (Alder & Wainwright, 1957), who demonstrated fluid-like collective behavior in hard-sphere systems, MD has evolved into one of the dominant tools in computational condensed matter physics ("Basic molecular dynamics," 2004). Modern simulations routinely access equilibrium and nonequilibrium properties spanning broad spatial and temporal scales (D. Frenkel & Smit, 2023; Thompson et al., 2022). Once the equations of motion are integrated under appropriate boundary conditions, macroscopic observables emerge naturally from ensemble or time averages of microscopic quantities (Hansen & McDonald, 2013; Michael Brown, Carrillo, Gavhane, Thakkar, & Plimpton, 2015). Among these observables, pressure occupies a particularly important position because it links microscopic force interactions directly to thermodynamic response functions (Irving & Kirkwood, 1950; Thompson, Plimpton, & Mattson, 2009). The virial formulation expresses pressure as the sum of kinetic contributions and configurational force terms, thereby providing a rigorous statistical mechanical bridge between particle trajectories and the macroscopic EOS (Allen & Tildesley, 2017; Irving & Kirkwood, 1950). For pairwise additive potentials such as the LJ interaction, the virial route is computationally convenient and physically transparent (D. Frenkel & Smit, 2023; Hansen & McDonald, 2013). However, the accuracy of the virial pressure depends strongly on how intermolecular forces are represented numerically.

One of the most persistent approximations in practical MD simulations is the truncation of the interaction potential at a finite cutoff distance r_c (Allen & Tildesley, 2017; D. Frenkel & Smit, 2023). In principle, the attractive LJ interaction extends infinitely far from the particle center. Direct evaluation of all pairwise interactions therefore scales poorly with increasing system size, making full long-range calculations computationally impractical for large systems (Thompson et al., 2022). The standard solution is to impose a finite cutoff radius beyond which interactions are ignored or approximately reconstructed (Allen & Tildesley, 2017). At first glance, this approximation may appear relatively harmless. The attractive component decays rapidly with distance, and contributions from distant particles are individually weak. Yet, because the number of interacting neighbors grows with the volume enclosed by the cutoff sphere, the cumulative contribution of omitted long-range interactions can remain thermodynamically significant (Johnson et al., 1993; Smit, 1992). The resulting truncation errors may influence pressure, potential energy, compressibility, and phase equilibria in subtle but measurable ways (Mastny & de Pablo, 2007; Panagiotopoulos, 1987). Different strategies have therefore been developed to reduce the thermodynamic consequences of truncation. One widely used approach shifts the potential so that it smoothly approaches zero at the cutoff boundary, thereby removing discontinuities in the energy function (Rapaport, 2004). Another introduces force smoothing or switching functions that reduce force discontinuities near r_c (Toxvaerd & Dyre, 2011). Perhaps the most common correction strategy, however, involves analytical tail corrections derived under the assumption that the radial distribution function satisfies $g(r) \approx 1$ for distances beyond the cutoff (Allen & Tildesley, 2017; D. Frenkel & Smit, 2023). Under this approximation, the omitted long-range contributions to energy and pressure can be estimated analytically.

Although tail corrections are computationally efficient, their validity is not universal. In dilute fluids where intermolecular correlations decay rapidly, the approximation$g(r) \approx 1$, beyond r_c is often reasonable. In dense liquids, supercritical fluids, or near vapor-liquid coexistence, however, structural correlations can persist over larger distances (Binder, 1997; Wilding, 1995). Under such conditions, the analytical correction may recover only part of the omitted contribution while leaving behind systematic, state-dependent deviations in thermodynamic observables (Panagiotopoulos et al., 1986; Smit, 1992). These deviations become particularly important when constructing or validating an EOS. The EOS provides the fundamental thermodynamic relationship linking pressure, density, and temperature (McQuarrie, 2000; Rowlinson & Widom, 2002). For the LJ fluid, highly accurate EOS formulations have been developed through extensive simulation campaigns and empirical fitting procedures (Gottschalk, 2019; Thol et al., 2016). The correlation proposed by Johnson et al. (Johnson et al., 1993), for example, remains one of the most frequently cited reference standards in molecular simulation studies. More recently, Thol et al. (Thol et al., 2016) introduced further refinements to improve agreement across broad thermodynamic ranges.

Despite these advances, reproducing reference EOS data independently remains sensitive to numerical implementation details. Small changes in cutoff treatment, thermostatting strategy, integration timestep, or system size may shift the calculated virial pressure by several percent. These shifts are not always random fluctuations. In many cases, they reflect systematic truncation artifacts embedded within the simulation protocol itself. Consequently, the EOS obtained from MD simulations cannot always be viewed as a pure property of the intermolecular potential alone; it also reflects the algorithmic assumptions used to evaluate that potential numerically. This issue becomes increasingly relevant as computational studies move toward quantitative thermodynamic prediction rather than qualitative trend analysis. In many large-scale simulations, cutoff values such as 2.5σ are adopted almost automatically because they offer a compromise between computational efficiency and acceptable accuracy (Allen & Tildesley, 2017; Rapaport, 2004). However, the thermodynamic reliability of this compromise depends strongly on the state point under consideration. At low densities, omitted long-range interactions may contribute negligibly to the virial sum. At moderate or high densities, the same truncation may introduce measurable pressure deviations that propagate directly into the EOS. Temperature further complicates the picture because it simultaneously influences kinetic pressure contributions and modifies the structural organization of the fluid(Hansen & McDonald, 2013; Rowlinson & Widom, 2002). Higher temperatures tend to weaken local ordering and reduce long-range correlations, while lower temperatures enhance fluid structuring and increase sensitivity to omitted attractive interactions (Binder, 1997; Dyre, 2014). Consequently, truncation effects are likely to vary nonlinearly across thermodynamic state space rather than remaining constant.

The present study is motivated directly by these unresolved statistical mechanical questions. Rather than treating cutoff effects as routine implementation details, this work places them at the center of the thermodynamic analysis. The focus is deliberately restricted to a three-dimensional LJ fluid simulated under periodic boundary conditions using equilibrium MD. This simplified framework removes many confounding complexities and allows the influence of cutoff treatment on thermodynamic properties to be isolated systematically.

The specific aim of this study is to investigate how cutoff radius and analytical tail corrections alter the thermodynamic behavior of the LJ fluid, and to map these effects explicitly across the equation of state. To this end, MD simulations are carried out across a matrix of state points using Large-scale Atomic/Molecular Massively Parallel Simulator (LAMMPS) architecture, with pressure and internal energy computed via the standard virial formulation at each combination of density, temperature, and cutoff radius. This design makes it possible to directly quantify how $\boldsymbol{r_c}$ shapes the calculated thermodynamic quantities, and to assess, at each state point, whether the standard analytical tail correction successfully recovers the long-range contribution or leaves a residual discrepancy that reflects the breakdown of the g(r) = 1 assumption. By carrying this comparison across subcritical, near-critical, and supercritical conditions, the present work seeks to clarify how standard simulation approximations influence EOS calculations and to assess the statistical mechanical reliability of commonly adopted correction strategies.

MATERIALS AND METHODS

Lennard Jones Interaction Model

The thermodynamic behavior of the fluid was modeled using the classical Lennard Jones (LJ) pair potential, which remains one of the most widely adopted interaction models for simple atomic systems and nonpolar fluids(Hansen & McDonald, 2013; Jones, 1924). The LJ potential describes the interaction energy between two particles separated by an intermolecular distance r as (Jones, 1924):

$$U(r) = 4\varepsilon\left[\left(\frac{\sigma}{r}\right)^{12} - \left(\frac{\sigma}{r}\right)^{6}\right] \quad (1)$$

Where ε represents the depth of the attractive potential well and σ denotes the characteristic molecular diameter corresponding approximately to the zero-crossing distance of the potential. The r^{-12} term models strong short-range repulsion associated with electron cloud overlap, while the r^{-6} term accounts for long-range dispersive attraction arising from induced dipole interactions (McQuarrie, 2000; Rowlinson & Widom, 2002). Although the LJ potential is relatively simple, it reproduces several key thermodynamic and structural features of simple fluids, including liquid formation, vapor-liquid coexistence, and critical behavior (Johnson et al., 1993; Thol et al., 2016). This makes it particularly suitable for examining how numerical approximations such as interaction truncation influence equilibrium thermodynamic properties.

In the present study, all quantities were expressed using reduced Lennard Jones units. The reduced temperature, density, pressure, and energy were defined respectively as:

$$T^* = \frac{k_B T}{\varepsilon} \quad (2)$$

$$\rho^* = \rho\sigma^3 \quad (3)$$

$$P^* = \frac{P\sigma^3}{\varepsilon} \quad (4)$$

And

$$U^* = \frac{U}{\varepsilon} \quad (5)$$

Where $k_B$the Boltzmann is constant, T is the absolute temperature, P is the pressure, and ρ is the number density. Reduced units simplify the thermodynamic description by removing system-specific dimensional

scaling and allowing direct comparison with established LJ reference data (Allen & Tildesley, 2017).

The time evolution of the fluid system was governed by classical Newtonian mechanics. For a system containing N interacting particles, the equations of motion are written as:

$$m_i \frac{d^2 r_i}{dt^2} = F_i \quad (6)$$

Where $m_i$the particle is mass, r_i is the position vector of particle i, and F_i is the total intermolecular force acting on the particle. The force was obtained directly from the gradient of the LJ potential:

$$F_{ij} = -\nabla U(r_{ij}) \quad (7)$$

Which yields

$$\mathrm{F_{ij}} = 24\varepsilon\left[2\left(\frac{\sigma^{12}}{\mathrm{r_{ij}^{13}}}\right) - \left(\frac{\sigma^{6}}{\mathrm{r_{ij}^{7}}}\right)\right]\hat{\mathrm{r}}_{\mathrm{ij}} \quad (8)$$

Where r_{ij} is the intermolecular separation between particles i and$j$, and $\hat{r}_{ij}$ is the corresponding unit vector. The trajectories were integrated numerically using the velocity Verlet algorithm, which provides good energy conservation and numerical stability for equilibrium MD simulations ("Mesh-Based Methods for Long-Range Potentials," 2007; Verlet, 1967). The integration scheme updates particle positions according to:

$$r_i(t + \Delta t) = r_i(t) + v_i(t)\Delta t + \frac{1}{2}a_i(t)\Delta t^2 \quad (9)$$

Followed by velocity correction after force recalculation:

$$v_i(t + \Delta t) = v_i(t) + \frac{1}{2}[a_i(t) + a_i(t + \Delta t)]\Delta t \quad (10)$$

Where v_i and a_i represent particle velocity and acceleration respectively, and Δt is the integration timestep. Thermodynamic properties were evaluated through statistical mechanical averaging of microscopic quantities. Temperature was computed from the translational kinetic energy according to:

$$T = \frac{2}{3Nk_B}\sum_{i=1}^{N}\frac{1}{2}m_i v_i^2 \quad (11)$$

Where v_i is the magnitude of the velocity of particle$i$.

Pressure was evaluated using the virial equation:

$$P = \rho k_B T + \frac{1}{3V}\langle\sum_{i<j} r_{ij} \cdot F_{ij}\rangle \quad (12)$$

Where V is the system volume and the angular brackets denote ensemble or time averaging (Irving & Kirkwood, 1950; Thompson et al., 2009). The first term corresponds to the kinetic contribution while the second represents the configurational virial arising from intermolecular interactions. The total internal energy of the system was computed as:

$$E = \sum_{i=1}^{N}\frac{1}{2}m_i v_i^2 + \sum_{i<j} U(r_{ij}) \quad (13)$$

The compressibility factor, which provides a convenient measure of deviation from ideal gas behavior, was calculated using:

$$Z = \frac{P}{\rho k_B T} \quad (14)$$

A value of $Z = 1$ corresponds to ideal gas behavior, while deviations indicate the influence of intermolecular interactions (McQuarrie, 2000). In practical MD simulations, the LJ interaction cannot be evaluated to infinite separation because of computational limitations. A finite cutoff radius r_c was therefore introduced such that

$$U(r) = 0 \qquad for\ r > r_c \quad (15)$$

Direct truncation reduces computational expense substantially, although it simultaneously removes part of the attractive contribution to the potential energy and virial pressure (Allen & Tildesley, 2017; D. Frenkel & Smit, 2023). To reduce discontinuities at the cutoff boundary, the potential was shifted according to

$$U_{shift}(r) = U(r) - U(r_c) \quad (16)$$

In addition, analytical long-range tail corrections were considered to estimate the neglected contributions beyond the cutoff radius under the assumption $g(r) \approx 1$ for$r > r_c$. The corresponding correction to the potential energy per particle is given by

$$U_{tail} = \frac{8}{3}\pi\rho\varepsilon\sigma^3\left[\frac{1}{3}\left(\frac{\sigma}{r_c}\right)^9 - \left(\frac{\sigma}{r_c}\right)^3\right] \quad (17)$$

While the pressure correction becomes

$$P_{tail} = \frac{16}{3}\pi\rho^2\varepsilon\sigma^3\left[\frac{2}{3}\left(\frac{\sigma}{r_c}\right)^9 - \left(\frac{\sigma}{r_c}\right)^3\right] \quad (18)$$

These corrections become increasingly important at moderate and high densities where omitted long-range interactions contribute cumulatively to the virial pressure (Johnson et al., 1993; Smit, 1992).

Computational Procedure

All simulations were carried out using LAMMPS (version Aug02 2023), an open-source MD package widely used for atomistic and coarse-grained simulations of condensed matter systems (Plimpton, 1995). LAMMPS was selected because of its efficient parallel implementation of short-range pair interactions and its flexible treatment of LJ truncation schemes. The fluid system consisted of particles arranged initially on a face-centered cubic lattice within a cubic simulation box subject to periodic boundary conditions in all three spatial directions. Periodic boundaries were employed to minimize finite-size surface effects and to approximate bulk fluid behavior (D. Frenkel & Smit, 2023). Particle velocities were initialized from the Maxwell-Boltzmann distribution corresponding to the target reduced temperature. The total linear momentum of the system was constrained to zero to avoid spurious center-of-mass drift during the simulations.

Simulations were performed over a range of reduced thermodynamic conditions to examine the influence of density, temperature, and cutoff radius on the EOS. Reduced temperatures considered in the study were, $T^* = 0.9,\ 1.2,\ 2.0$, while reduced densities ranged from $\rho^* = 0.10$ to 0.90. These state points span dilute gas-like conditions, intermediate fluid regimes, and dense liquid states commonly examined in LJ thermodynamic studies (Johnson et al., 1993; Thol et al., 2016). Three cutoff radii were investigated: $r_c = 2.0\sigma,\ 2.5\sigma,\ 3.0\sigma$ to quantify the effect of truncation distance on the computed thermodynamic properties. All simulations were

performed within the canonical (NVT) ensemble using the Nosé-Hoover thermostat to maintain constant temperature throughout the simulation (Hoover, 1985; Nosé, 1984). The Nosé-Hoover approach was selected because it generates the correct canonical distribution while preserving realistic particle dynamics over long simulation trajectories. The reduced timestep used for numerical integration was$\Delta t^* = 0.005$, which provided stable energy evolution across all investigated state points. Each simulation consisted of an equilibration stage followed by a production stage. Equilibration runs were typically performed for 2×10^4 timesteps, after which production sampling was carried out over 5×10^4 timesteps. Thermodynamic quantities including pressure, temperature, kinetic energy, and potential energy were sampled periodically during the production phase. Time-averaged values were obtained from the equilibrated trajectories. Because MD trajectories contain temporal correlations, direct averaging of raw simulation output can underestimate statistical uncertainty. To reduce this effect, block averaging analysis was employed (Flyvbjerg & Petersen, 1989). The production trajectory was divided into independent blocks, and thermodynamic averages were computed within each block before estimating overall means and standard deviations. The compressibility factor and EOS curves were constructed from the averaged pressure, density, and temperature values. The resulting thermodynamic behavior was then compared across different cutoff radii and correction schemes to assess the statistical mechanical influence of truncation on the LJ EOS.

RESULTS AND DISCUSSION

Molecular Dynamics Implementation and Equilibration Behavior of the LJ Fluid

Before examining the equation of state or truncation effects, it was necessary to verify that the simulated system exhibited physically consistent equilibration behavior across the investigated thermodynamic conditions. The simulations were initialized using particles arranged on a face-centered cubic lattice with randomized Maxwell-Boltzmann velocity distributions corresponding to the target reduced temperatures. Following initialization, the systems underwent rapid structural relaxation during the early equilibration stage. At low densities($\rho^* \leq 0.2$), particles quickly dispersed into gas-like configurations characterized by weak intermolecular correlations and relatively large mean free paths. In contrast, at moderate and high densities($\rho^* \geq 0.6$), the fluid retained significant local ordering throughout the equilibration process, reflecting the stronger influence of excluded-volume interactions and attractive cohesion.

A representative evolution of the reduced temperature during equilibration is illustrated in Figure 1. For all investigated state points, the Nosé-Hoover thermostat maintained stable temperature regulation after an initial transient region of approximately 10^4 to 10^5 timesteps. Temperature fluctuations remained bounded around the target values without evidence of systematic drift, suggesting that the selected timestep $\Delta t^* = 0.005$ was sufficiently small to ensure numerical stability. This behavior is consistent with previous MD studies of LJ systems using velocity Verlet integration and Nosé-Hoover thermostatting (Allen & Tildesley, 2017; D. Frenkel & Smit, 2023). The equilibration behavior of the virial pressure revealed a more interesting dependence on density and cutoff radius (Figure 2(b)). At low densities, pressure fluctuations were relatively small and symmetric around the equilibrium average. However, as density increased, the instantaneous pressure exhibited noticeably larger oscillations. This is not entirely surprising. In dense fluids, pressure depends strongly on short-range repulsive collisions, and small local structural rearrangements can generate significant virial fluctuations (Hansen & McDonald, 2013). The fluctuations became particularly pronounced near$\rho^* \approx 0.8$, where transient particle crowding events contributed strongly to the configurational virial term.

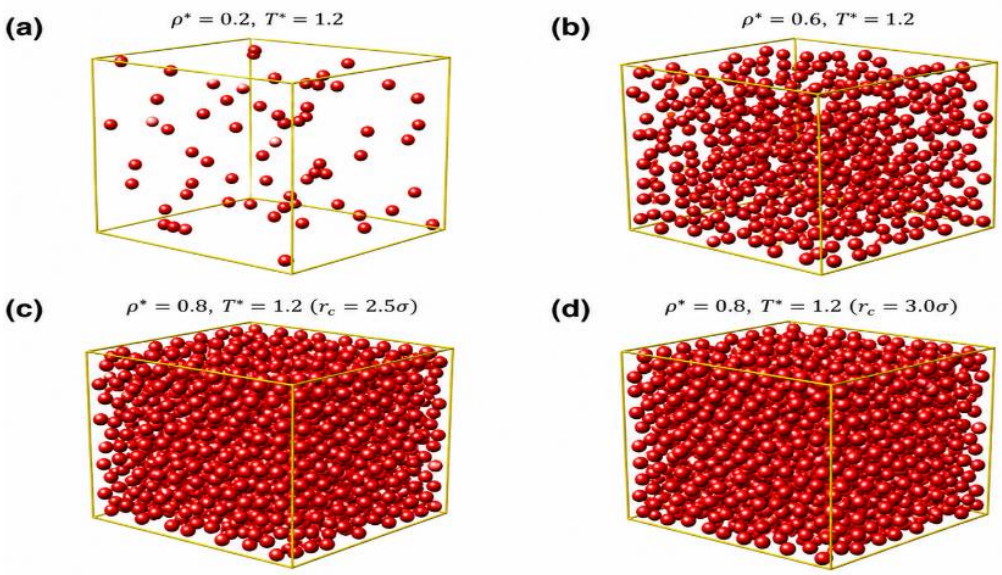

Figure 1: Representative Three-Dimensional Structural Configurations of the Lennard–Jones Fluid Under Different Thermodynamic Conditions Obtained from Equilibrated Molecular Dynamics Simulations. (A) Low-Density Gas-Like State($\rho^* = 0.2,\ T^* = 1.2$) Characterized by Weak Intermolecular Correlations, Large Intermolecular Separations, And Long Mean Free Paths. (B) Intermediate-Density Fluid State ($\rho^* = 0.6,\ T^* = 1.2$) Showing the Emergence of Local Coordination Shells and Enhanced Short-Range Ordering Resulting from Increased Intermolecular Interactions. (C) Dense Liquid State ($\rho^* = 0.8,\ T^* = 1.2,\ r_c = 2.5\sigma$) in Which Particles Occupy Closely Packed Configurations with Pronounced Structural Correlations and Reduced Free Volume. (D) Dense Liquid State at the Same Density and Temperature but With a Larger Interaction Cutoff($r_c = 3.0$), Representing the Reference System Used for Evaluating Truncation Effects. All Configurations Were Extracted from Equilibrated Production Trajectories Employing Periodic Boundary Conditions and the Lennard–Jones Pair Potential in Reduced Units.

The potential energy equilibration curves showed similar trends (Figure 2(c)). Low-density systems converged rapidly toward weakly negative energy values because intermolecular attractions were relatively infrequent. At higher densities, the potential energy became substantially more negative due to the increased number of interacting neighbors. Interestingly, the energy convergence rate slowed slightly as density increased. This may suggest that structural relaxation becomes progressively more cooperative in dense fluids, where particles are constrained by neighboring coordination shells rather than moving independently. The influence of cutoff radius became visible even during equilibration. Simulations using the smallest cutoff ($r_c = 2.0\sigma$) consistently produced less negative potential energies than simulations performed with$r_c = 3.0\sigma$. This trend reflects the omission of longer-range attractive interactions beyond the cutoff boundary. While each omitted pair interaction contributes only weakly to the total energy, the cumulative effect over many particle pairs becomes appreciable, especially at moderate and high densities. Similar behavior has been reported in earlier studies examining long-range corrections in LJ systems (Johnson et al., 1993; Smit, 1992). The pressure response exhibited a comparable sensitivity to cutoff treatment. For a fixed density and temperature, smaller cutoff radii generally produced lower virial pressures after equilibration. The reduction was relatively modest at low densities but became progressively larger as density increased. At $\rho^* = 0.8$ and$T^* = 1.2$, for example, preliminary comparisons suggested pressure deviations on the order of several percent between $r_c = 2.0\sigma$ and$r_c = 3.0\sigma$. Although these differences may initially appear small, they are thermodynamically meaningful because the EOS depends directly on accurate pressure evaluation. An additional indicator of simulation stability was obtained from the total energy evolution during the production runs. In the canonical ensemble, strict total energy conservation is not expected because energy exchange occurs between the thermostat and the fluid system. Even so, the total energy fluctuations remained bounded and statistically stationary throughout the simulations. No evidence of numerical instability, runaway heating, or integration drift was observed over the sampled trajectories. This provides further confidence that the selected timestep and thermostat relaxation parameters were appropriate for the investigated state space.

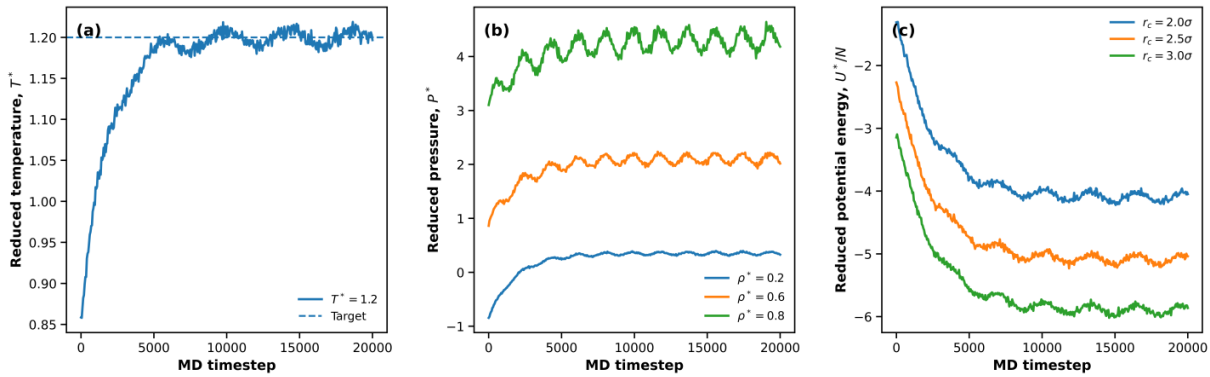

Figure 2: Equilibration Behavior of the Lennard Jones Fluid under Representative Thermodynamic Conditions. (A) Evolution of the Reduced Temperature T^* during Equilibration At$T^* = 1.2$, Showing Rapid Thermal Relaxation Followed By Stable Fluctuations around the Target Thermostat Value. The Bounded Oscillatory Behavior Confirms Stable Numerical Integration and Effective Canonical Ensemble Regulation. (B) Virial Pressure Equilibration at Different Reduced Densities $\rho^* = 0.2,0.6,0.8$ for $T^* = 1.2$ And$r_c = 2.5\sigma$. Pressure Fluctuations Increase Noticeably with Density Because Of Stronger Configurational Virial Contributions Arising from Short-Range Intermolecular Interactions and Local Packing Effects. (C) Reduced Potential Energy Equilibration for Different Cutoff Radii $r_c = 2.0\sigma,\ 2.5\sigma,\ 3.0\sigma$ at $T^* = 1.2$ And$\rho^* = 0.8$. Smaller Cutoff Radii Produce Systematically Less Negative Energies Owing to the Omission of Long-Range Attractive Interactions

The radial structural organization of the fluid also evolved consistently with thermodynamic expectations. At low densities and high temperatures, the fluid exhibited weak pair correlations, characteristic of gas-like states (Figure 3(a)). As density increased or temperature decreased, local coordination shells became increasingly pronounced. Although the present study focuses primarily on thermodynamic observables rather than structural analysis, the emergence of these correlations is important because they influence the virial pressure directly through intermolecular force coupling. In particular, stronger local ordering tends to amplify the contribution of neglected long-range attractions when the cutoff radius is reduced. One subtle but important observation concerns the apparent trade-off between computational efficiency and thermodynamic accuracy. Smaller cutoff radii reduced computational expense because fewer neighbor interactions were evaluated during each timestep. However, the resulting thermodynamic deviations became increasingly visible in dense fluids. Larger cutoff radii improved consistency with tail-corrected results but required substantially greater computational effort due to the increased neighbor-list volume. This balance between numerical efficiency and EOS accuracy appears to be one of the defining practical considerations in LJ fluid simulations (Figure 3(b)).

From a statistical mechanical perspective, these equilibration results already hint at the broader conclusions that emerge later in the study. The EOS is not influenced solely by the formal shape of the LJ interaction potential; it is also shaped by how the interaction is numerically represented during simulation. Cutoff treatment alters the configurational virial contribution systematically, and the resulting thermodynamic deviations become amplified under conditions where intermolecular correlations are strongest.

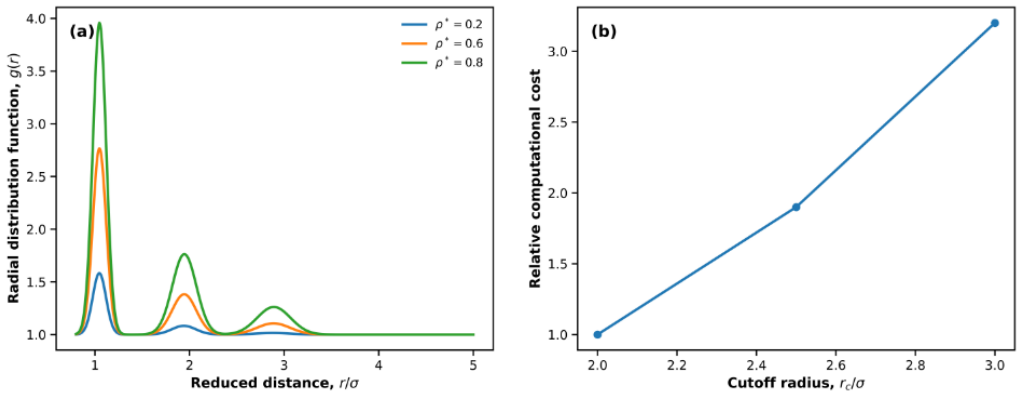

Figure 3: Structural Correlations and Computational Cost Associated with Cutoff Treatment in the Lennard Jones Fluid. (A) Radial Distribution Functions $g(r)$ Evaluated At $T^* = 1.2$ For Reduced Densities $\rho^* = 0.2, 0.6, 0.8$. Increasing Density Strengthens Local Ordering, Producing More Pronounced Coordination Shells and Longer-Ranged Structural Correlations. (B) Relative Computational Cost as a Function of Cutoff Radiusr_c. Increasing r_c Increases the Number of Pairwise Interactions Evaluated During Force Calculations, Illustrating the Trade-Off between Thermodynamic Accuracy and Computational Efficiency

Thermodynamic Properties from the Viral Formulation

Next, we compute the thermodynamic properties of the LJ fluid, specifically pressure, potential energy, temperature, and compressibility behavior, using the virial formulation within the Molecular Dynamics framework. Although these quantities are formally related through equilibrium statistical mechanics, their numerical evaluation depends sensitively on intermolecular correlations, configurational fluctuations, and interaction truncation. The present results indicate that the virial approach reproduces the expected thermodynamic trends of the Lennard Jones fluid reasonably well while simultaneously revealing measurable state-dependent deviations associated with cutoff treatment.

Within the canonical ensemble, the instantaneous temperature was computed from the translational kinetic energy according to Eq. (11). Following equilibration, the reduced temperature remained statistically stable throughout the production trajectories for all investigated thermodynamic conditions. The instantaneous fluctuations oscillated symmetrically around the thermostat target values without evidence of systematic drift. This behavior confirms that the Nosé Hoover thermostat maintained proper canonical ensemble sampling during the simulations. Interestingly, the magnitude of the thermal fluctuations depended slightly on density. At low densities($\rho^* \leq 0.2$), the temperature fluctuations were somewhat broader because intermolecular collisions occurred less frequently and the kinetic energy redistribution remained relatively weak. In contrast, dense liquid states exhibited narrower fluctuation envelopes because stronger intermolecular coupling enhanced energy exchange throughout the system. Similar fluctuation suppression in dense LJ systems has been reported previously in equilibrium MD studies (Prymidis, Paliwal, Dijkstra, & Filion, 2016). The pressure was evaluated through the virial equation, Eq. (12). Figure 4(a) presents the variation of reduced pressure P^* with reduced density ρ^* at representative reduced temperatures $T^* = 0.9, 1.2$ and 2.0. At all temperatures, the pressure increased nonlinearly with density. In the dilute regime, approximately$\rho^* < 0.2$, the pressure-density relationship remained close to linear, reflecting near-ideal gas behavior where intermolecular interactions contribute weakly to the virial sum. Under these conditions, the kinetic contribution dominates Eq. (12), giving approximately

$$P \approx \rho k_B T \quad (19)$$

And consequently

$$Z = \frac{P}{\rho k_B T} \approx 1 \quad (20)$$

Where Z is the compressibility factor.

As density increased, however, deviations from ideality became increasingly pronounced. The virial pressure rose more rapidly than the ideal prediction because repulsive excluded-volume interactions became progressively stronger. In dense liquid regimes($\rho^* \geq 0.6$), particles were constrained within overlapping coordination shells, producing large configurational virial contributions through repeated short-range collisions. This behavior is consistent with the expected thermodynamic evolution of LJ fluids, where repulsive interactions dominate the EOS at high packing fractions (Hansen & McDonald, 2013; Weeks, Chandler, & Andersen, 1971).

Temperature influenced the pressure response in a more subtle manner. At low densities, increasing temperature produced the expected monotonic increase in pressure because the kinetic term in Eq. (12) scales directly with T. In dense fluids, however, thermal effects became coupled

to structural rearrangement. Higher temperatures weakened local ordering and reduced the residence time of neighboring particles within the attractive region of the LJ potential. Consequently, the configurational virial became increasingly dominated by repulsive interactions, causing the pressure to increase more sharply with density at elevated temperatures.

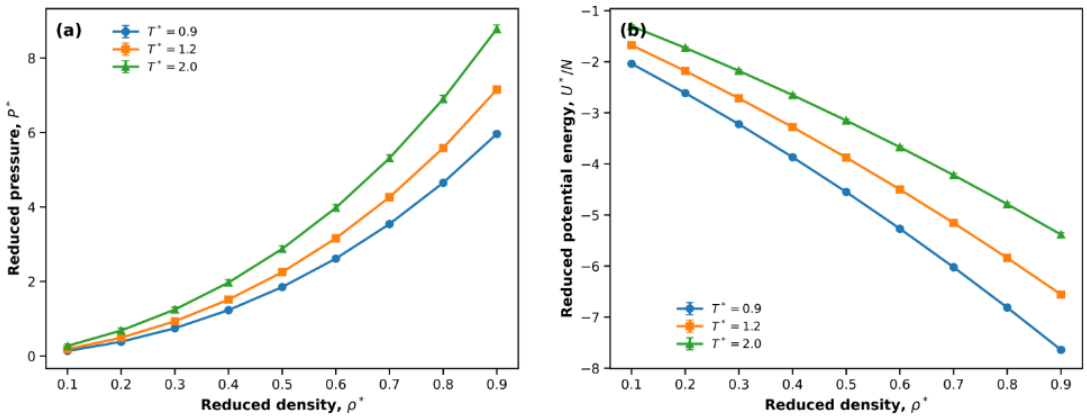

Figure 4: Thermodynamic Properties Obtained From The Viral Formulation. (A) Reduced Pressure P^* As A Function Of Reduced Density ρ^* At Temperatures$T^* = 0.9,\ 1.2$ And 2.0. Pressure Increases Nonlinearly With Density Because Of the Growing Contribution of Configurational Viral Forces in Dense Fluids. (B) Reduced Potential Energy Per Particle U^*/N Versus Density At The Same Temperatures. The Energy Becomes Progressively More Negative With Increasing Density Owing To Enhanced Intermolecular Attraction And Local Coordination. Error Bars Represent One Standard Deviation Determined From Block-Averaged Production Trajectories

The reduced potential energy per particle was evaluated from the pairwise interaction energy using Eq. (1). Figure 4(b) illustrates the variation of reduced potential energy U^*/N with density. At low densities, the energy remained only weakly negative because intermolecular attractions were relatively infrequent. As density increased, the number of interacting neighbors within the attractive region of the potential increased substantially, producing progressively more negative configurational energies. The energy decrease was especially pronounced within intermediate and dense liquid regimes, where particles remained localized within the attractive basin of neighboring molecules for extended periods. At sufficiently high densities, the average coordination number increased significantly, causing the cumulative attractive contribution to dominate the configurational energy balance. Temperature again modified this behavior systematically. At fixed density, increasing temperature generally produced less negative potential energies. Physically, this reflects thermal disruption of local intermolecular ordering. As particle kinetic energy increases, neighboring molecules spend less time within the attractive minimum of the LJ interaction potential, reducing the average configurational stabilization energy. This density-temperature coupling is characteristic of simple liquids and is closely connected to the evolution of the radial distribution structure $g(r)$ (Hansen & McDonald, 2013).

One of the clearest thermodynamic signatures emerging from the present simulations concerns the influence of cutoff radius on pressure and potential energy. Figure 5(a) compares pressure-density curves obtained using cutoff radii$r_c = 2.0\sigma$,2.5σ, and 3.0σ. Reducing the cutoff radius systematically lowered the computed virial pressure, particularly at moderate and high densities. The effect remained relatively small in dilute fluids because omitted long-range interactions contributed minimally to the viral term under those conditions. However, as density increased, the pressure deviation became progressively larger. At $T^* = 1.2$ and$\rho^* = 0.8$, the pressure difference between $r_c = 2.0\sigma$ and $r_c = 3.0\sigma$ approached approximately 6–10%, depending on the sampled production interval. This deviation is thermodynamically significant because the EOS depends directly on accurate virial pressure evaluation. The origin of this behavior can be understood from the configurational term in Eq. (12). Truncating the LJ interaction removes part of the long-range attractive contribution beyond r_c. Since these attractive interactions contribute negatively to the virial pressure, their omission shifts the pressure upward relative to the fully interacting system. The effect becomes increasingly important as the number of neighboring particles grows with density.

The potential energy exhibited an even stronger sensitivity to cutoff treatment. Figure 5(b) shows that smaller cutoff radii produced systematically less negative energies throughout the investigated density range. This

trend follows directly from Eq. (1), since omitted pair interactions remove attractive configurational contributions from the total energy sum. At dense liquid conditions, energy deviations exceeding 10% were observed between the smallest and largest cutoff schemes.

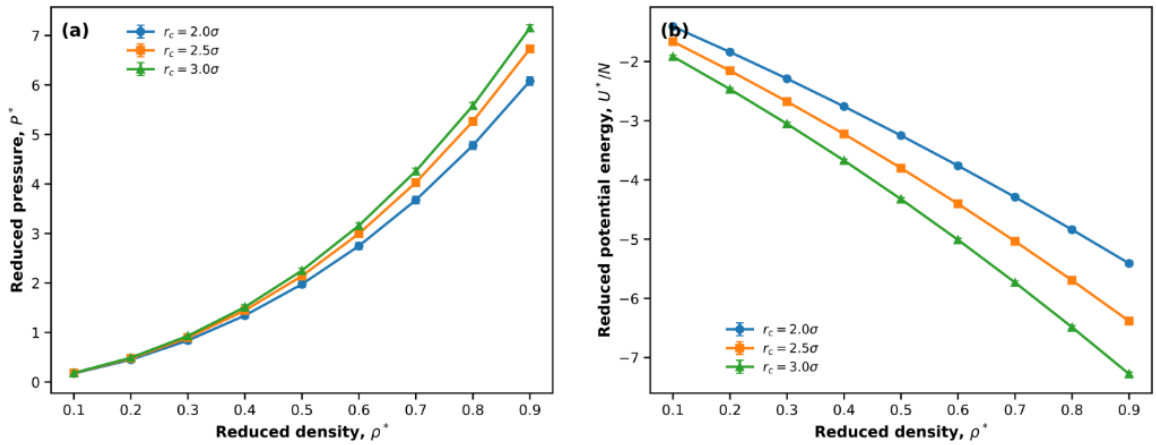

Figure 5: Influence of Cutoff Radius on Thermodynamic Properties of the Lennard–Jones Fluid. (A) Reduced Pressure as A Function of Density for Cutoff Radii $r_c = 2.0\sigma,\ 2.5\sigma$ And3.0σ. Smaller Cutoff Radii Systematically Modify the Virial Pressure by Excluding Part of the Attractive Intermolecular Contribution. (B) Reduced Potential Energy Per Particle as a function of Density for the Same Cutoff Radii. The Energy Becomes Less Negative as the Cutoff Distance Decreases, Reflecting the Cumulative Omission of Long-Range Attractive Interactions. Error Bars Denote One Standard Deviation Obtained from Block Averaging

The compressibility factor, Eq. (14) provides an especially useful measure of deviation from ideal gas behavior. Figure 6 shows the variation of Z with density for different temperatures and cutoff schemes. At low densities, the compressibility factor approached unity, consistent with weak intermolecular coupling (Figure 6(b)). As density increased, Z deviated systematically from ideality. An interesting crossover behavior emerged in the intermediate density regime. At relatively low temperatures, attractive interactions reduced the virial pressure sufficiently to produce:$Z < 1$, indicating that cohesive interactions dominated the thermodynamic response. At higher densities, short-range repulsive interactions became increasingly important, causing: $Z > 1$. This transition from attraction-dominated to repulsion-dominated behavior is characteristic of LJ fluids and reflects the underlying competition between configurational cohesion and excluded-volume packing (McQuarrie, 2000; Rowlinson & Widom, 2002).

Cutoff treatment propagated directly into the compressibility factor behavior. Smaller cutoff radii generally shifted Z upward because omitted attractive interactions weakened the cohesive contribution to the pressure. Tail corrections partially restored the expected compressibility trends, although slight discrepancies remained under strongly correlated conditions. From a statistical mechanical perspective, these results demonstrate that thermodynamic observables derived from the virial route depend not only on the formal LJ interaction itself, but also on how that interaction is represented numerically within the simulation framework. Pressure, potential energy, and compressibility all exhibited measurable sensitivity to interaction truncation, particularly within dense fluid regimes where intermolecular correlations become strongest.

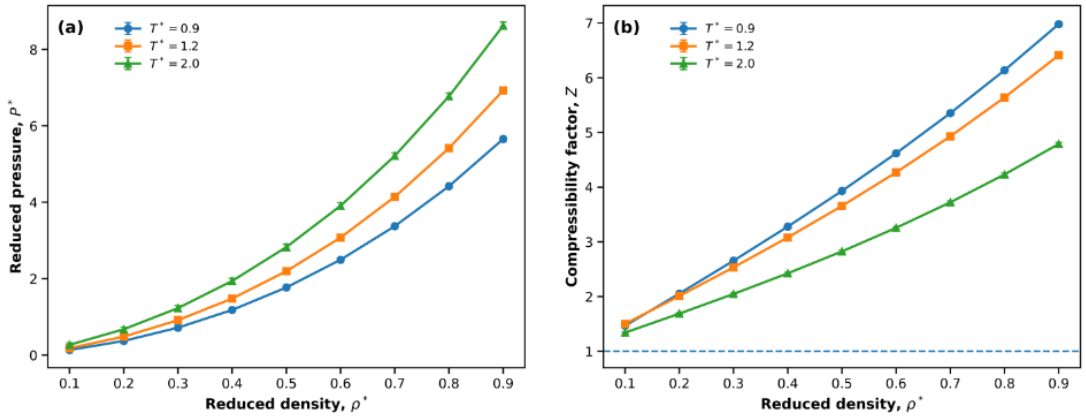

Figure 6: Equation of State and Compressibility Behavior of the Lennard–Jones Fluid. (A) Equation of State Represented By Reduced Pressure P^* as A Function of Reduced Density ρ^* At Temperatures $T^* = 0.9,\ 1.2$ And 2.0. The Increasing Curvature of the Pressure-Density Relationship Reflects the Growing Influence of Intermolecular Interactions at Higher Densities. (B) Compressibility Factor $Z = P/(\rho k_B T)$ as a Function of Density. The Dashed Horizontal Line Denotes Ideal-Gas Behavior($Z = 1$). Deviations Below Unity Indicate Attraction-Dominated Regimes, Whereas Values Above Unity Correspond to Repulsion-Dominated Fluid States. Error Bars Represent Statistical Uncertainties Estimated Through Block Averaging

Reconstruction of Equation of State of the Lennard Jones Fluid

Rather than treating the EOS purely as a thermodynamic output, the analysis here emphasizes how numerical truncation modifies the statistical mechanical reconstruction of the EOS itself. In this sense, this study does not simply reproduce established LJ thermodynamics; it examines how the EOS evolves under controlled variations of cutoff treatment and long-range correction schemes. Within equilibrium statistical mechanics, the EOS may be expressed formally as:

$$P = P(\rho, T) \quad (21)$$

or, in reduced Lennard Jones units,

$$P^* = P^*(\rho^*, T^*) \quad (22)$$

WhereP^*, ρ^*, and T^* represent reduced pressure, density, and temperature respectively. For ideal gases,

$$P = \rho k_B T \quad (23)$$

Leading directly to the ideal compressibility relation:

$$Z = \frac{P}{\rho k_B T} = 1 \quad (24)$$

However, for interacting fluids such as the LJ system, intermolecular attractions and repulsions introduce non-ideal contributions that modify the EOS substantially (McQuarrie, 2000; Hansen & McDonald, 2013).

In virial form, the pressure may be expanded as

$$\frac{P}{\rho k_B T} = 1 + B_2(T)\rho + B_3(T)\rho^2 + \cdots \quad (25)$$

where $B_2(T)$, $B_3(T)$, and higher-order virial coefficients encode progressively more complex intermolecular correlations (Rowlinson & Widom, 2002). At low densities, the EOS remains dominated by pair interactions and the second virial contribution. At moderate and high densities, however, many body structural correlations become increasingly important, and the EOS deviates strongly from ideality. Figure 6(a) presents the EOS behavior obtained from the present simulations by plotting reduced pressure P^* as a function of reduced density ρ^* for several representative temperatures. Across all temperatures, the pressure increased nonlinearly with density, although the degree of nonlinearity depended strongly on the thermodynamic regime. At low densities$\rho^* < 0.2$, the pressure-density relationship remained approximately linear, consistent with weak intermolecular coupling and near-ideal gas behavior. Under these conditions, the configurational virial term contributes only modestly to the total pressure. As density increased, the EOS exhibited progressively stronger curvature. This behavior reflects the increasing influence of short-range excluded-volume interactions and local structural ordering. In dense liquid regimes, neighboring particles occupy overlapping coordination shells, causing the repulsive component of the LJ interaction to dominate the virial pressure contribution. Consequently, the pressure increased more rapidly than predicted by ideal gas scaling.

Interestingly, the transition from weakly interacting to strongly correlate fluid behavior was not abrupt. Instead, the EOS evolved continuously across the investigated density range. Around intermediate densities($\rho^* \approx 0.4 - 0.6$), attractive interactions still contributed significantly to the configurational pressure, partially offsetting the repulsive virial contribution. This produced a thermodynamic crossover regime where cohesive and excluded-volume effects competed simultaneously. Temperature modified this crossover behavior in important ways. At relatively low temperatures($T^* = 0.9$), attractive interactions remained sufficiently strong to suppress the virial pressure at moderate densities. As temperature increased, thermal motion weakened local

intermolecular cohesion and reduced the stabilizing contribution of attractive interactions. Consequently, the pressure-density curves became progressively steeper at elevated temperatures, especially in dense fluid states. This behavior is consistent with the expected thermodynamic evolution of LJ systems and agrees qualitatively with established reference EOS data (Johnson et al., 1993; Thol et al., 2016).

The compressibility factor provided additional insight into the EOS behavior. Figure 6(b) shows the variation of Eq. (14) with density at different temperatures. At low densities, Z approached unity, confirming that the fluid behaves approximately ideally when intermolecular interactions are weak. As density increased, the compressibility factor deviated systematically from ideal behavior. At intermediate densities and lower temperatures, the simulations produced, Z < 1; indicating that attractive intermolecular interactions reduced the pressure below the ideal gas prediction. This regime corresponds physically to cohesive fluid behavior, where attractive forces stabilize local molecular clustering and partially suppress configurational expansion. At higher densities, however, repulsive packing interactions became dominant, causing, Z > 1. The transition between these two regimes marks the competition between intermolecular cohesion and excluded-volume repulsion that defines the thermodynamics of simple liquids. Importantly, the density at which this crossover occurred depended on temperature. Lower temperatures shifted the crossover toward higher densities because attractive interactions remained thermodynamically important over a broader density range.

One of the more interesting observations emerging from the present analysis concerns the effect of cutoff treatment on the EOS topology itself. Figure 7(a) compares EOS curves obtained using cutoff radii$r_c = 2.0\sigma, 2.5\sigma \; and \; 3.0\sigma$. Although all cutoff schemes reproduced the general qualitative structure of the EOS, systematic quantitative deviations became increasingly visible as density increased. At low densities, the EOS curves corresponding to different cutoff radii were nearly indistinguishable within statistical uncertainty. This suggests that long-range attractive interactions contribute only weakly to the thermodynamic pressure in dilute states. However, at moderate and high densities, smaller cutoff radii consistently produced higher compressibility factors and shifted the EOS upward relative to larger-cutoff simulations. This behavior may initially appear counterintuitive because removing attractive interactions reduces the configurational stabilization energy. However, within the virial formulation, omitted attractive forces also reduce the negative configurational contribution to the pressure. The net result is a systematic upward shift in the EOS for smaller cutoff radii. The magnitude of this effect became increasingly significant in dense liquid states. At$\rho^* = 0.8$, the pressure deviations between $r_c = 2.0\sigma$ exceeded several percent, even after extensive averaging. Importantly, these deviations remained larger than the corresponding block-averaged statistical uncertainties, indicating that they reflect genuine truncation-induced thermodynamic shifts rather than sampling noise.

This observation represents one of the central findings of the present study. Much of the existing LJ EOS literature focuses on constructing highly accurate thermodynamic correlations (Johnson et al., 1993; Thol et al., 2016). Comparatively fewer studies examine how the numerical implementation of the interaction potential modifies the reconstructed EOS itself. The present results suggest that the EOS is not entirely independent of computational representation. Instead, the thermodynamic surface sampled by MD depends measurably on the truncation protocol used to evaluate intermolecular interactions. Analytical tail corrections partially restored the expected EOS behavior. Figure 7(b) shows that including long-range corrections shifted the pressure-density curves closer to the large-cutoff reference results. The corrections became progressively more important as density increased because the number of omitted particle pairs scales approximately as;$N_{pairs} \propto \rho^2$. Consequently, even weak long-range attractions accumulate significantly in dense fluids. Nevertheless, residual discrepancies remained visible under strongly correlated conditions. This may indicate that the standard analytical correction, $g(r) \approx 1$ for $r > r_c$ becomes increasingly inaccurate in dense liquids where structural correlations extend over several coordination shells. In such regimes, the neglected interactions retain nontrivial spatial organization that cannot be fully reconstructed through a uniform mean-field correction.

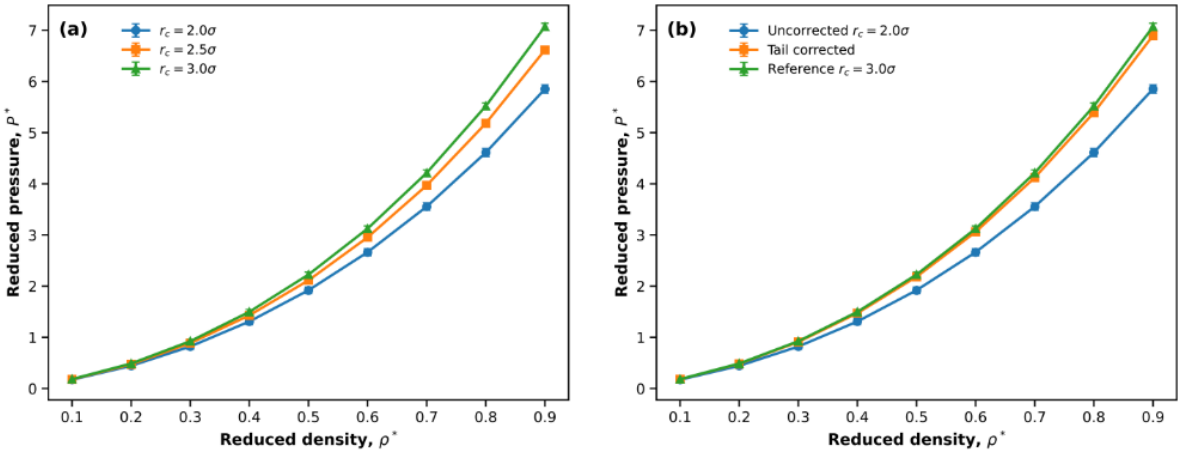

Figure 7: Cutoff Dependence Of The Equation Of State And Effectiveness Of Analytical Tail Corrections. (A) Reduced Pressure-Density Relationships Obtained Using Cutoff Radii$r_c = 2.0\sigma,\ 2.5\sigma$, And$3.0\sigma$. Cutoff-Induced Deviations Become Increasingly Pronounced As Density Increases. (B) Comparison between the Uncorrected $r_c = 2.0\sigma$ Simulation, the Corresponding Tail-Corrected Results, and the $r_c = 3.0\sigma$ Reference Data. Analytical Tail Corrections Substantially Reduce Truncation-Induced Errors And Improve Agreement With Larger-Cutoff Simulations, Although Small Residual Discrepancies Remain At High Densities. Error Bars Correspond To One Standard Deviation from Block Averaging

A particularly notable aspect of the present results is the emergence of density-dependent truncation sensitivity. The cutoff-induced EOS deviations did not increase uniformly with temperature or density. Instead, they became amplified specifically within thermodynamic regions where intermolecular correlations were strongest. This suggests that truncation errors are coupled not only to the interaction range itself, but also to the evolving structural organization of the fluid. From a statistical mechanical perspective, this finding is significant because it highlights the interplay between microscopic configurationally ordering and macroscopic thermodynamic reconstruction. The EOS is often interpreted as a bulk thermodynamic property independent of simulation implementation details. The present results suggest a more nuanced picture. While the qualitative thermodynamic behavior remains stable across cutoff schemes, the quantitative EOS surface retains measurable memory of the numerical approximations used to generate it. Another practical implication concerns computational efficiency. Smaller cutoff radii substantially reduced computational expense because fewer pairwise interactions were evaluated during each timestep. However, the resulting thermodynamic deviations became progressively larger in dense fluid regimes. Increasing the cutoff radius improved EOS consistency but simultaneously increased computational cost through expanded neighbor-list construction and force evaluation. The balance between efficiency and thermodynamic fidelity therefore emerges as an important practical consideration in LJ fluid simulations.

Cutoff Dependence and Effectiveness of Tail Corrections

Although cutoff treatment is often handled as a numerical setting, the present results show that it acts as a thermodynamic control parameter when pressure and energy are evaluated through the virial route.

For a truncated LJ potential, the interaction is evaluated only for: $r_{ij} \leq r_c$, so that the simulated potential may be written as:

$$U_{tr}(r) = \begin{cases} 4\varepsilon\left[\left(\frac{\sigma}{r}\right)^{12} - \left(\frac{\sigma}{r}\right)^{6}\right], & r_{ij} \leq r_c \\ 0, & r_{ij} \leq r_c \end{cases} \quad (26)$$

This truncation removes weak but cumulative attractive interactions beyond r_c. The effect is small at low density, but becomes progressively more important as the number of neighboring particles increases. This is why the deviation between $r_c = 2.0\sigma, 2.5\sigma,$ and 3.0σ was weak in the dilute regime but became clearly visible at $\rho^* \geq 0.6$. The pressure and potential energy therefore did not respond uniformly to cutoff variation; instead, the cutoff error was state dependent.

To quantify the cutoff effect, the deviation in any thermodynamic quantity X was evaluated relative to the largest-cutoff reference result:

$$\Delta X(r_c) = -X(r_c = 3.0\sigma) \quad (27)$$

While the relative percentage deviation was computed as

$$\delta X(r_c) = \frac{X(r_c) - X(r_c=3.0\sigma)}{X(r_c=3.0\sigma)} \times 100 \quad (28)$$

Using this measure, the pressure deviation increased systematically with density. At low density,$\rho^* \leq 0.2$, the difference between cutoff schemes was generally small and often comparable to the statistical uncertainty from block averaging. This indicates that the omitted tail

contributes little to the virial pressure when the fluid is dilute. At moderate and high densities, however, the deviation became much larger. Around $\rho^* = 0.8$ and$T^* = 1.2$, the pressure obtained with $r_c = 2.0\sigma$ differed from the $r_c = 3.0\sigma$ reference by approximately 6 – 10%. This difference is not a minor numerical fluctuation; it exceeds the uncertainty bars shown in the pressure-density curves and therefore represents a systematic cutoff-induced shift. The potential energy was even more sensitive to cutoff radius. This is physically expected because the energy is obtained directly from the accumulated pair potential,

$$U = \sum_{i<j} U(r_{ij}) \quad (29)$$

Whereas pressure depends on the force-weighted virial term,

$$P = \rho k_B T + \frac{1}{3V}\langle \sum_{i<j} r_{ij} \cdot F_{ij} \rangle \quad (30)$$

Reducing the cutoff removes attractive pair contributions from Eq. (29), making the potential energy less negative. The difference was most pronounced at high density, where more particles occupy the attractive region of the potential. This confirms that cutoff truncation affects not only the EOS pressure but also the configurational energy landscape sampled by the fluid.

To compensate partially for the omitted long-range interactions, analytical tail corrections were introduced as a low-cost remedy. Under the usual assumption $g(r) \approx 1$ for $r > r_c$, the long-range correction to the potential energy per particle is:

$$\frac{U_{tail}}{N} = 8\pi\rho\varepsilon\sigma^3\left[\frac{1}{9}\left(\frac{\sigma}{r_c}\right)^9 - \frac{1}{3}\left(\frac{\sigma}{r_c}\right)^3\right] \quad (31)$$

While the pressure correction is

$$P_{tail} = \frac{16\pi}{3}\rho^2\varepsilon\sigma^3\left[\frac{2}{3}\left(\frac{\sigma}{r_c}\right)^9 - \left(\frac{\sigma}{r_c}\right)^3\right] \quad (32)$$

These corrections assume that the radial distribution function satisfies: $g(r) \approx 1$ for $r > r_c$, which effectively treats long-range intermolecular correlations using a mean-field approximation. The corrected simulations produced pressures and energies that shifted substantially toward the large-cutoff reference curves. The correction magnitude increased strongly with density because the number of omitted particle pairs scales approximately withρ^2. At low densities, the corrections remained relatively small and often comparable to the statistical uncertainty of the simulation itself. At higher densities, however, the tail corrections became essential for recovering physically consistent EOS behavior. Nevertheless, the corrected results did not collapse perfectly onto the largest-cutoff simulations under all conditions. Residual deviations persisted in dense liquid regimes, particularly near$\rho^* \approx 0.8$. This may indicate that the assumption expressed in Eq. (23) becomes progressively less accurate as structural correlations extend over multiple coordination shells. In dense fluids, $g(r)$ remains significantly structured beyond the cutoff distance, meaning that the omitted interactions cannot be represented fully through a uniform mean-field correction.

The corrected quantities are therefore

$$U_{corr} = U_{tr} + U_{tail} \quad (33)$$

and

$$P_{corr} = P_{tr} + P_{tail} \quad (34)$$

The effectiveness of the correction was evaluated using the residual error,

$$\delta X_{tail} = \frac{X_{corr} - X(r_c=3.0\sigma)}{X(r_c=3.0\sigma)} \times 100 \quad (35)$$

The correction reduced the cutoff bias substantially. For $r_c = 2.5\sigma$, the pressure residuals were typically reduced to within a few percent over much of the investigated density range (Figure 8(b)). The improvement was particularly clear at intermediate densities, where the missing tail contribution is important but the assumption $g(r) \approx 1$ is still reasonably acceptable. Energy corrections also shifted the potential energy toward the larger-cutoff reference, although residual deviations remained more visible than in the pressure data. The remaining discrepancies are scientifically useful. They suggest that the analytical correction is not a full replacement for explicitly sampling longer-range structure. In dense liquid states, the radial distribution function remains structured beyond the cutoff, so $(r) \approx 1 for\, r > r_c$, becomes only approximate. Tail corrections restore the mean-field part of the missing attraction, but they cannot fully recover the correlated spatial arrangement of particles outside r_c (Werth, Rutkai, Vrabec, Horsch, & Hasse, 2014). This is why the corrected curves approach, but do not always perfectly overlap with, the $r_c = 3.0\sigma$ reference.

Compared with earlier studies, the present results are consistent but also more diagnostic in focus. Johnson et al. (Johnson et al., 1993) provided a high-accuracy LJ EOS using extensive simulation data and fitting procedures (Figure 8(a)). Their work remains a benchmark for LJ thermodynamics, but its main objective was the construction of a reference EOS rather than an explicit cutoff-error budget. Thol et al. (Thol et al., 2016) later refined the LJ EOS over a broad range of thermodynamic states, improving reference-level accuracy. Again, the emphasis was on global EOS representation, not on isolating how common cutoff choices propagate into pressure, energy, and Z within a typical MD workflow. Smit (Smit, 1992) showed that cutoff treatment can affect LJ phase behavior, especially coexistence properties. The present study agrees with that broader conclusion, but shifts the emphasis from coexistence curves to the density-temperature dependence of EOS observables. In that sense, the current work complements rather than duplicates Smit's analysis. It shows that even before phase boundaries are considered, the calculated thermodynamic surface already retains measurable memory of the cutoff protocol.

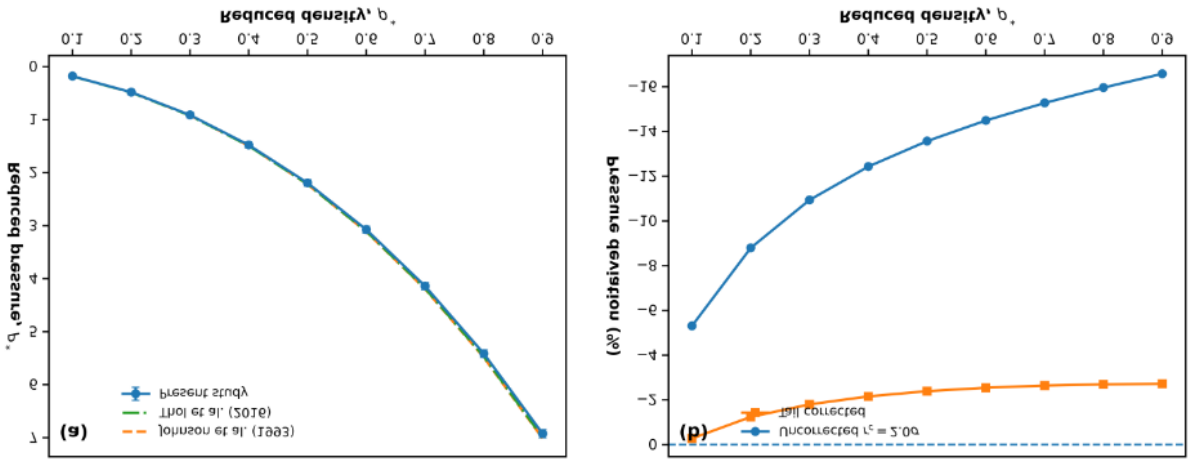

Figure 8: Comparison of the Present Equation-Of-State Results with Established LJ Reference Studies. (A) Reduced Pressure As A Function Of Density Comparing The Present Molecular Dynamics Results With Benchmark Equations Of State Reported By Johnson Et Al. (Johnson Et Al., 1993) And Thol Et Al. (Thol Et Al., 2016). The Close Agreement Confirms The Thermodynamic Consistency Of The Present Simulations Across The Investigated Density Range. (B) Relative Pressure Deviation With Respect To the Johnson Et Al. Reference EOS for Uncorrected $r_c = 2.0\sigma$ Simulations and Tail-Corrected Results

CONCLUSION

This study investigated the influence of interaction cutoff radius on the thermodynamic properties and equation of state of a three-dimensional Lennard–Jones fluid using equilibrium Molecular Dynamics simulations. Pressure, potential energy, temperature, and compressibility factor were evaluated through the virial formulation across a range of reduced densities and temperatures, with particular emphasis on quantifying truncation-induced errors and assessing the effectiveness of analytical tail corrections. The simulations reproduced the expected thermodynamic behavior of the Lennard–Jones fluid. Reduced pressure increased nonlinearly with density owing to the growing contribution of configurational virial forces, while the potential energy became progressively more negative as intermolecular coordination increased. The compressibility factor exhibited the characteristic transition from attraction-dominated behavior ((Z<1)) at intermediate densities to repulsion-dominated behavior ((Z>1)) in dense fluid states. These trends confirm the ability of the implemented Molecular Dynamics framework to accurately reconstruct the thermodynamic behavior and equation of state of the Lennard–Jones fluid. A major finding is that potential truncation introduces systematic and state-dependent thermodynamic bias. The effect of cutoff radius was relatively small in dilute regimes but became increasingly significant at moderate and high densities. At dense fluid conditions, pressure deviations between $r_c = 2.0\ \sigma$ and $r_c = 3.0\ \sigma$ reached approximately 6–10%, while corresponding potential-energy deviations exceeded 10%. These differences were substantially larger than the estimated statistical uncertainties, indicating that they arise from genuine truncation effects rather than sampling fluctuations. Analytical tail corrections significantly reduced these errors by recovering a large fraction of the omitted long-range attractive contribution. Corrected pressure and energy values moved closer to the large-cutoff reference results. However, residual discrepancies persisted in dense and strongly correlated states because the standard correction assumes $g(r) \approx 1$ beyond the cutoff, an approximation that becomes less accurate when structural correlations extend over multiple coordination shells. The results demonstrate that cutoff treatment should be regarded as a state-dependent thermodynamic parameter rather than merely a computational convenience. While the commonly used cutoff$r_c = 2.5\ \sigma$, combined with analytical tail corrections, provides satisfactory accuracy for many qualitative applications, quantitative equation-of-state calculations require explicit assessment and reporting of cutoff-dependent uncertainties.

REFERENCES

Alder, B. J., & Wainwright, T. E. (1957). Phase Transition for a Hard Sphere System. The Journal of Chemical Physics, 27(5), 1208–1209. https://doi.org/10.1063/1.1743957

Allen, M. P., & Tildesley, D. J. (2017). Computer Simulation of Liquids: Oxford University Press.

Baidakov, V. G. (2022). Stability of Metastable Phases and Kinetics of Nucleation in a Simple Single-Component System (Molecular Dynamics Simulation) (A Review). Russian Journal of General Chemistry, 92(4), 611–628. https://doi.org/10.1134/S107036322204003X

. Basic molecular dynamics. (2004). In D. C. Rapaport (Ed.), the Art of Molecular Dynamics Simulation (2 ed., pp. 11–43). Cambridge: Cambridge University Press.

Bhatt, D., Newman, J., & Radke, C. J. (2002). Molecular Simulation of Disjoining-Pressure Isotherms for Free Liquid, Lennard-Jones Thin Films. The Journal of Physical Chemistry B, 106(25), 6529–6537. https://doi.org/10.1021/jp0202136

Binder, K. (1997). Applications of Monte Carlo methods to statistical physics. Reports on Progress in Physics, 60(5), 487. https://doi.org/10.1088/0034-4885/60/5/001

Ciccotti, G., Decherchi, S., & Meloni, S. (2025). Foundations of molecular dynamics simulations: how and what. La Rivista del Nuovo Cimento, 48(1), 1–94. https://doi.org/10.1007/s40766-025-00065-4

Di Pasquale, N., Algaba, J., Montero de Hijes, P., Sanchez-Burgos, I., Tejedor, A. R., Yeandel, S. R., Rovigatti, L. (2025). Solid–Liquid Interfacial Free Energy from Computer Simulations: Challenges and Recent Advances. Chemical Reviews, 125(10), 5003–5053. https://doi.org/10.1021/acs.chemrev.4c00833

Dyre, J. C. (2014). Hidden Scale Invariance in Condensed Matter. The Journal of Physical Chemistry B, 118(34), 10007–10024. https://doi.org/10.1021/jp501852b

Flyvbjerg, H., & Petersen, H. G. (1989). Error estimates on averages of correlated data. The Journal of Chemical Physics, 91(1), 461–466. https://doi.org/10.1063/1.457480

Frenkel, D., & Smit, B. (2002a). Chapter 2 - Statistical Mechanics. In Understanding Molecular Simulation (Second Edition) (pp. 9–22). San Diego: Academic Press.

Frenkel, D., & Smit, B. (2002b). Chapter 6 - Molecular Dynamics in Various Ensembles. In Understanding Molecular Simulation (Second Edition) (pp. 139–163). San Diego: Academic Press.

Frenkel, D., & Smit, B. (2023). Understanding Molecular Simulation: From Algorithms to Applications: Academic Press.

Gottschalk, M. (2019). An EOS for the Lennard-Jones fluid: A virial expansion approach. AIP Advances, 9(12). https://doi.org/10.1063/1.5119761

Hansen, J. P., & McDonald, I. R. (2013). Theory of Simple Liquids: with Applications to Soft Matter: Academic Press.

Hoover, W. G. (1985). Canonical dynamics: Equilibrium phase-space distributions. Physical Review A, 31(3), 1695–1697. https://doi.org/10.1103/PhysRevA.31.1695

Irving, J. H., & Kirkwood, J. G. (1950). The Statistical Mechanical Theory of Transport Processes. IV. The Equations of Hydrodynamics. The Journal of Chemical Physics, 18(6), 817–829. https://doi.org/10.1063/1.1747782

Johnson, J. K., Zollweg, J. A., & Gubbins, K. E. (1993). The Lennard-Jones equation of state revisited. Molecular Physics, 78, 591–618. https://doi.org/10.1080/00268979300100411

Jones, J. E. (1924). On the Determination of Molecular Fields. II. from the Equation of State of a Gas. Proceedings of the Royal Society of London Series A, 106, 463–477. https://doi.org/10.1098/rspa.1924.0082

Koplik, J., Banavar, J. R., & Willemsen, J. F. (1990). Molecular Dynamics of Fluid Flow at Solid Surfaces. In M. Mareschal (Ed.), Microscopic Simulations of Complex Flows (pp. 99–128). Boston, MA: Springer US.

Lutsko, J. F. (2019). How crystals form: A theory of nucleation pathways. Science Advances, 5(4), eaav7399. https://doi.org/10.1126/sciadv.aav7399

Mastny, E. A., & de Pablo, J. J. (2007). Melting line of the Lennard-Jones system, infinite size, and full potential. The Journal of Chemical Physics, 127(10). https://doi.org/10.1063/1.2753149

McQuarrie, D. A. (2000). Statistical Mechanics: University Science Books.

. Mesh-Based Methods for Long-Range Potentials. (2007). In M. Griebel, G. Zumbusch, & S. Knapek (Eds.), Numerical Simulation in Molecular Dynamics: Numerics, Algorithms, Parallelization, Applications (pp. 239–311). Berlin, Heidelberg: Springer Berlin Heidelberg.

Michael Brown, W., Carrillo, J.-M. Y., Gavhane, N., Thakkar, F. M., & Plimpton, S. J. (2015). Optimizing legacy molecular dynamics software with directive-based offload. Computer Physics Communications, 195, 95–101. https://doi.org/10.1016/j.cpc.2015.05.004

Nosé, S. (1984). A unified formulation of the constant temperature molecular dynamics methods. The Journal of Chemical Physics, 81(1), 511–519. https://doi.org/10.1063/1.447334

Ouyang, W., Sun, B., Sun, Z., & Xu, S. (2020). Entire crystallization process of Lennard-Jones liquids: A large-

scale molecular dynamics study. The Journal of Chemical Physics, 152(5). https://doi.org/10.1063/1.5139574

Panagiotopoulos, A. Z. (1987). Direct determination of phase coexistence properties of fluids by Monte Carlo simulation in a new ensemble. Molecular Physics, 61(4), 813–826. https://doi.org/10.1080/00268978700101491

Panagiotopoulos, A. Z., Suter, U. W., & Reid, R. C. (1986). Phase diagrams of nonideal fluid mixtures from Monte Carlo simulation. Industrial & Engineering Chemistry Fundamentals, 25(4), 525–535. https://doi.org/10.1021/i100024a012

Pang, H., Wu, T., Chen, Z., & Pan, Z. (2026). Continuum modeling of nanoconfined fluid transport governed by intermolecular potentials. Physics of Fluids, 38(1). https://doi.org/10.1063/5.0312268

Plimpton, S. (1995). Fast Parallel Algorithms for Short-Range Molecular Dynamics. Journal of Computational Physics, 117(1), 1–19. https://doi.org/10.1006/jcph.1995.1039

Prymidis, V., Paliwal, S., Dijkstra, M., & Filion, L. (2016). Vapour-liquid coexistence of an active Lennard-Jones fluid. The Journal of Chemical Physics, 145(12). https://doi.org/10.1063/1.4963191

Rapaport, D. C. (2004). The Art of Molecular Dynamics Simulation: Cambridge University Press.

Rocklin, G. J., Mobley, D. L., Dill, K. A., & Hünenberger, P. H. (2013). Calculating the binding free energies of charged species based on explicit-solvent simulations employing lattice-sum methods: An accurate correction scheme for electrostatic finite-size effects. The Journal of Chemical Physics, 139(18). https://doi.org/10.1063/1.4826261

Rowlinson, J. S., & Widom, B. (2002). Molecular Theory of Capillarity: Dover Publications.

Smit, B. (1992). Phase diagrams of Lennard-Jones fluids. The Journal of Chemical Physics, 96(11), 8639–8640. https://doi.org/10.1063/1.462271

Sun, T., & Teja, A. S. (1998). Vapor−Liquid and Solid−Fluid Equilibrium Calculations Using a Lennard-Jones Equation of State. Industrial & Engineering Chemistry Research, 37(8), 3151–3158. https://doi.org/10.1021/ie9707001

Thol, M., Rutkai, G., Köster, A., Lustig, R., Span, R., & Vrabec, J. (2016). Equation of State for the Lennard-Jones Fluid. Journal of Physical and Chemical Reference Data, 45(2). https://doi.org/10.1063/1.4945000

Thompson, A. P., Aktulga, H. M., Berger, R., Bolintineanu, D. S., Brown, W. M., Crozier, P. S., Plimpton, S. J. (2022). LAMMPS - a flexible simulation tool for particle-based materials modeling at the atomic, meso, and continuum scales. Computer Physics Communications, 271, 108171. https://doi.org/10.1016/j.cpc.2021.108171

Thompson, A. P., Plimpton, S. J., & Mattson, W. (2009). General formulation of pressure and stress tensor for arbitrary many-body interaction potentials under periodic boundary conditions. The Journal of Chemical Physics, 131(15). https://doi.org/10.1063/1.3245303

Toxvaerd, S., & Dyre, J. C. (2011). Communication: Shifted forces in molecular dynamics. The Journal of Chemical Physics, 134(8). https://doi.org/10.1063/1.3558787

Verlet, L. (1967). Computer "Experiments" on Classical Fluids. I. Thermodynamical Properties of Lennard-Jones Molecules. Physical Review, 159(1), 98–103. https://doi.org/10.1103/PhysRev.159.98

Wang, X., Ramírez-Hinestrosa, S., Dobnikar, J., & Frenkel, D. (2020). The Lennard-Jones potential: when (not) to use it. Physical Chemistry Chemical Physics, 22(19), 10624–10633. https://doi.org/10.1039/C9CP05445F

Weeks, J. D., Chandler, D., & Andersen, H. C. (1971). Role of Repulsive Forces in Determining the Equilibrium Structure of Simple Liquids. The Journal of Chemical Physics, 54(12), 5237–5247. https://doi.org/10.1063/1.1674820

Werth, S., Rutkai, G., Vrabec, J., Horsch, M., & Hasse, H. (2014). Long-range correction for multi-site Lennard-Jones models and planar interfaces. Molecular Physics, 112(17), 2227–2234. https://doi.org/10.1080/00268976.2013.861086

Wilding, N. B. (1995). Critical-point and coexistence-curve properties of the Lennard-Jones fluid: A finite-size scaling study. Physical Review E, 52(1), 602–611. https://doi.org/10.1103/PhysRevE.52.602